

Oxidation of Electron-Deficient Phenols Mediated by Hypervalent Iodine(V) Reagents: Fundamental Mechanistic Features Revealed by a DFT-Based Investigation

Mona Jalali,^a Alex C. Bissember,^a Brian F. Yates,^a Sarah E. Wengryniuk,^{*b} and Alireza Ariafard,^{*a}

^a School of Natural Sciences – Chemistry, University of Tasmania, Hobart, Tasmania 7001, Australia

^b Department of Chemistry, Temple University, Philadelphia 19122, USA

ABSTRACT

Hypervalent iodine(V) (HVI) compounds are highly efficient reagents for the double oxidative dearomatization of electron-rich phenols to *o*-quinones. We recently reported that an underexplored class of iodine(V) reagents possessing bidentate bipyridine ligands, termed Bi(*N*)-HVIs, could efficiently dearomatize electron-poor phenols for the first time. To better understand the fundamental mechanistic basis of this unique reactivity, density functional theory (DFT) was utilized. In this way, different pathways were explored to determine why Bi(*N*)-HVIs are capable of facilitating these challenging transformations while more traditional hypervalent species, such as IBX cannot. Our calculations reveal that the first redox process is the rate-determining step, the barrier of which hinges on the identity of the ligands bound to the iodine(V) center. This crucial process is composed of three steps: (a) ligand exchange, (b) hypervalent twist, and (c) reductive elimination. We found that strong coordinating ligands disfavor these elementary steps and, for this reason, HVIs bearing such ligands cannot oxidize the electron-poor phenols. In contrast, the weakly coordinating triflate ligands in Bi(*N*)-HVIs allow for the kinetically favorable oxidation of such phenols {e.g., $\Delta G^\ddagger = \sim 22$ kcal/mol where Bi(*N*) = Bi(4-CO₂Et**ipy**)}. It was also identified that trapping triflic acid, which is generated *in situ*, is a key role played by the basic bidentate bipyridine ligands in Bi(*N*)-HVIs as this serves to minimize decomposition of the sensitive *ortho*-quinone product.

Keywords

Density functional theory (DFT); phenol oxidation, bidentate nitrogen ligand, hypervalent iodine reagents, *ortho*-quinone, reaction mechanism

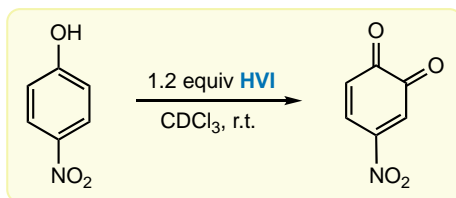
INTRODUCTION

Hypervalent iodine (HVI) compounds represent a class of important and versatile reagents and reactants in organic synthesis.¹ For example, iodine(V) species, such as 2-iodoxybenzoic acid (IBX), are recognized as effective oxidants for a wide range of synthetic transformations.² More specifically, the double oxidation of phenols by IBX or related iodine(V) reagents delivers *ortho*-quinones in a highly regioselective manner.³ However, to date, a notable limitation of iodine(V)-mediated phenol oxidation chemistry is that these transformations are typically restricted to electron-rich phenol substrates.

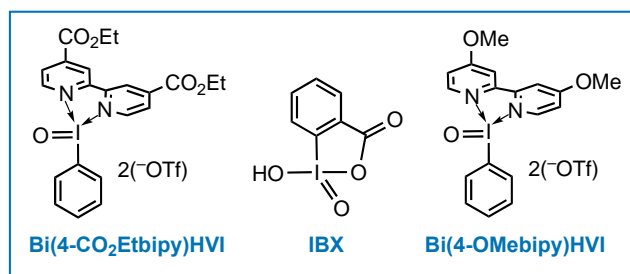
Bidentate nitrogen-ligated iodine(V) compounds, Bi(*N*)-HVIs, were first reported by Zhdankin and coworkers in 2002.⁴ Recently, we demonstrated that these compounds, and specifically Bi(*4-CO₂Et*bipy)-HVI, were uniquely effective at facilitating the highly efficient double oxidative dearomatization of electron-deficient phenols, such as *p*-nitrophenol (Table 1, entries 1 and 2).⁵ In this report, the reactivity of Bi(*4-CO₂Et*bipy)-HVI was benchmarked against a range of other iodine(V) reagents. Specifically, IBX provided very low yields of the target quinone and precursor PhI(O)(OAc)₂ gave no reaction at all (entries 3 and 4). The stronger oxidant PhI(O)(OTf)₂ afforded the product quinone in 59% yield after 20 minutes, which decreased to 27% yield after 4 hours due to continued oxidative degradation (entries 5 and 6). Interestingly, Bi(*4-OMe*Etbipy)-HVI provided the product in much lower yields in comparison to Bi(*4-CO₂Et*bipy)-HVI (entry 7). This revealed that electronic effects within the bipyridine ligand might play a crucial role in the efficiency of the oxidation. It was also interesting to note that the reaction employing pyridine-ligated PhI(O)(Py)₂(OTf)₂ only returned unreacted

starting material, indicating a bidentate ligand may also be required for desired dearomatization.

Table 1. Reported dearomatization of electron-deficient phenols to *ortho*-quinones by various iodine(V) reagents: selected results.⁵



entry	HVI oxidant	time (h)	yield (%)
1	Bi(4-CO ₂ Et bi py)HVI	0.5	99
2	Bi(4-CO ₂ Et bi py)HVI	4	91
3	IBX	24	12
4	PhI(O)(OAc) ₂	24	0
5	PhI(O)(OTf) ₂	0.66	59
6	PhI(O)(OTf) ₂	4	27
7	Bi(4-OMe bi py)HVI	0.66	38
8	PhI(O)(Py) ₂ (OTf) ₂	0.66	0



The above-mentioned experimental results prompted us to comprehensively investigate the mechanism of the oxidation of *p*-nitrophenol by the above-mentioned iodine(V) oxidants with the aim of answering the following questions: (i) Why are Bi(4-CO₂Et**bi**py)-HVI and PhI(O)(OTf)₂ potent oxidants in this chemistry, while IBX and PhI(O)(OAc)₂ are not? (ii) Is there a difference between the reactivity of Bi(4-CO₂Et**bi**py)-HVI compared to PhI(O)(OTf)₂? (iii) If not, why is the reaction efficiency for the former greater than that for the latter? (iv) Why does the replacement of Bi(4-CO₂Et**bi**py)-HVI with Bi(4-OMe**bi**py)-HVI considerably

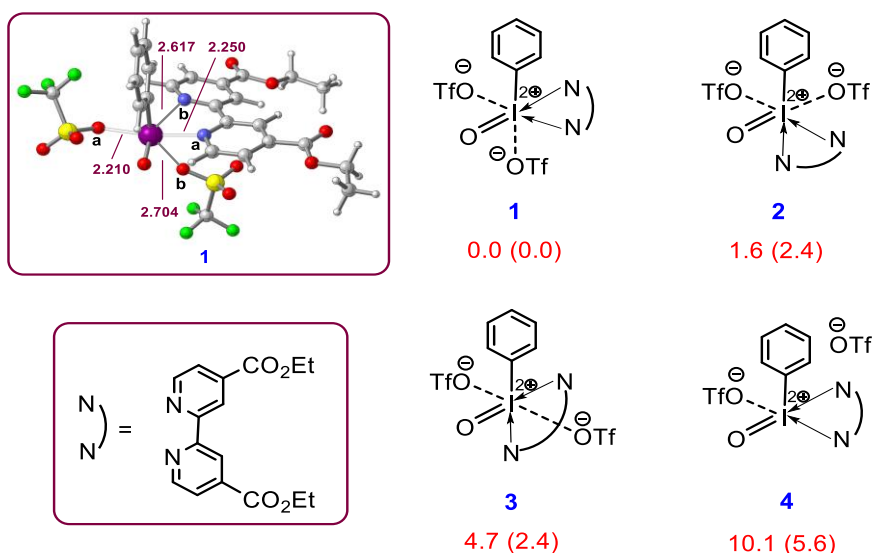
decrease the product yield? Why does the use of pyridine rather than a bipyridine attenuate the reactivity of the iodine(V) reagent? We anticipated that employing Density Functional Theory (DFT) to answer the foregoing questions would provide an enhanced understanding of the fundamental processes involved in iodine(V)-mediated oxidations. Furthermore, by revealing how the structure of Bi(*4-CO₂Et*bipy)-HVI specifically relates to its function, we thought that our study could serve as a platform from which the design of new hypervalent iodine(V) reagents and associated organic transformations would be better enabled.

RESULTS AND DISCUSSION

We commenced our DFT investigation by evaluating the stability of different isomers of Bi(*4-CO₂Et*bipy)-HVI. The four lower energy isomers of Bi(*4-CO₂Et*bipy)-HVI are shown in Figure 1a. This found that structure **1**, with a distorted octahedral geometry, is the most stable of these. In this complex, the oxo, bipyridine ligand, and a triflate anion occupy equatorial positions, while the second triflate occupies the axial position *trans* to the phenyl ligand. It is worth noting that due to the strong *trans* influence of the phenyl ligand, the iodine center binds more weakly to the axial triflate than to the equatorial triflate. This is reflected in the longer I–O^b bond distance within **1**. Similarly, the strong *trans* influence of the oxo ligand results in unsymmetrical coordination of bipyridine, which is consistent with the longer distance between the I and N^b atoms in comparison to the I and N^a atoms. Other isomers are less stable than **1** by 1.6 kcal/mol (isomer **2**), 4.7 kcal/mol (isomer **3**), and 10.1 kcal/mol (isomer **4**). The lower stability of five-coordinate ion pair **4** compared to other isomers indicates that the triflate ligand *trans* to the phenyl is more likely to remain bound to the iodine center (although weakly). We also found that the most stable structure **1** is resistant to complete dissociation of the bipyridine and triflate ligands. This is supported by the predicted endergonicity of these processes (Figure 1b). The same is true for other isomers (see Figures S1 and S2).

A recent study investigating the stability of isomers of a related Bi(*bipy*)-HVI species also found that an isomer structure analogous to structure **1** is the most stable.⁶ This consistency suggests that regardless of the electronic nature of the bidentate nitrogen ligand, isomer **1** is likely lower in energy than the other possible systems.

(a)



(b)

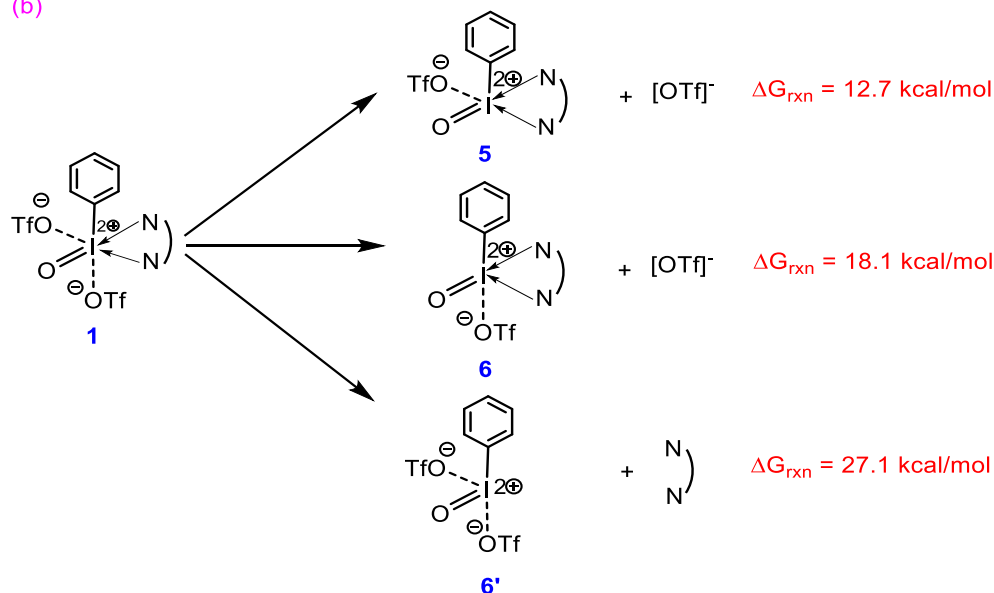
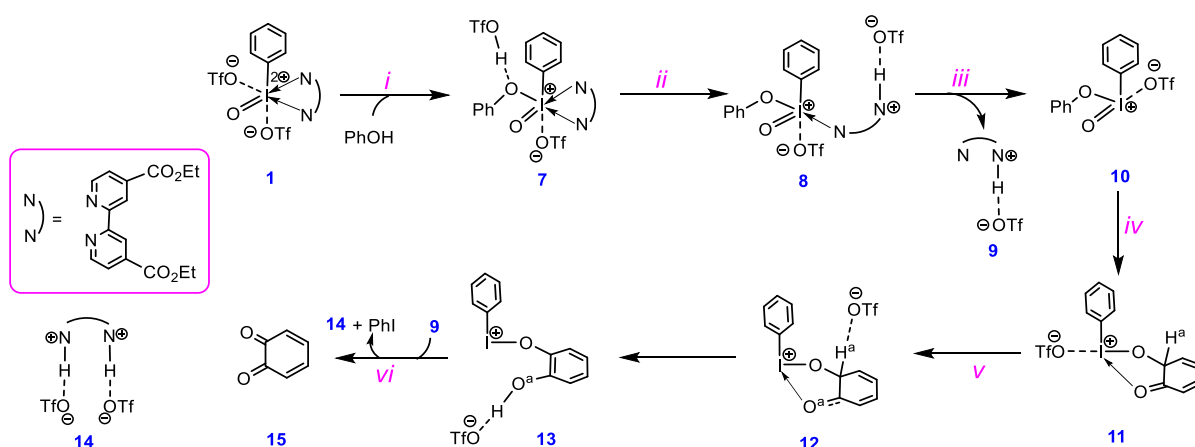


Figure 1. (a) Stability of different isomers of Bi(4-CO₂Etbipy)-HVI. (b) Reaction free energies for dissociation of the triflate and bipyridine ligands from **1**. Free energies calculated by SMD/M06-2X/def2-TZVP//SMD/M06-2X/LANL2DZ(d),6-31G(d) in chloroform are given in kcal/mol.

Oxidation of *p*-nitrophenol by Bi(*bipy*)-HVI. Next, we focused on understanding why Bi(4-

CO_2Et bipy)-HVI is a suitable reagent for oxidation of electron-deficient phenols in contrast to IBX (Table 1, entries 1 and 3).⁵ To this end, different mechanistic pathways were explored for the oxidation of PhOH by Bi($4-CO_2Et$ bipy)-HVI, the results of which are given in the Supporting Information (see Figures S3 and S4). Scheme 1 outlines the most favorable pathway for the phenol oxidation identified from our DFT studies. This reaction involves the following key steps: (i) ligand exchange between phenol and Bi($4-CO_2Et$ bipy)-HVI, giving adduct **7** stabilized by *in-situ*-generated triflic acid; (ii) formation of complex **8** via addition of triflic acid to the bipyridine ligand; (iii) generation of intermediate **10**, obtained by the dissociation of **9** from **8**, followed by an isomerization; (iv) the first redox process; (v) tautomerization assisted by the triflate ligand via sequence **11** \rightarrow **12** \rightarrow **13**; and, finally, (vi) the second redox process that forms *ortho*-quinone **15**.



Scheme 1. Key steps for phenol oxidation mediated by **1** derived from our DFT investigation.

Figure 2 shows the energy profile calculated for oxidative dearomatization of *p*-nitrophenol as a model for an electron-deficient substrate based on the mechanism outlined in Scheme 1. Accordingly, the reaction commences by formation of hydrogen-bonded adduct **16**, followed by a ligand exchange involving the concerted interchange associative (CIA) mechanism⁷ through transition structure **TS**₁₆₋₁₇ to provide adduct **17** which is stabilized by a hydrogen bonding interaction between *in-situ*-generated triflic acid and the phenolate ligand. This step is

calculated to occur with an activation barrier of around 11 kcal/mol and is endergonic by about 8 kcal/mol. Following this, the resulting triflic acid protonates the bipyridine nitrogen *trans* to the oxo ligand (N^b) in a thermodynamically favorable process to give intermediate **19**. Due to the π conjugation within the bipyridine ligand, the addition of the proton to N^b significantly reduces the basicity of N^a and, thus, it binds less strongly to the iodine(V) center in **19**. This is consistent with the longer I–N^a distance in **19** (2.426 Å) than in **18** (2.356 Å) (Figure 2). In other words, N^b protonation reduces the coordinative stability of the iodine(V) molecule and it changes from a rather inert to a more labile complex.⁸ The dissociation of **9** from **19** produces **20** in a thermoneutral fashion which then isomerizes to more stable structure **21_OTf**. Since the phenolate provides a weaker *trans* influence relative to the phenyl, the triflate binds more strongly to the iodine atom in **21_OTf**, resulting in this complex being more stable than **20**. This is consistent with the shorter I–OTf bond distance within **21_OTf** (2.252 Å) in comparison to the equivalent bond in **20** (2.412 Å) (Figure 2). It is established that a hypervalent twist must take place for the iodine oxidant to be sufficiently reactive toward the redox process.^{9,10} The corresponding twist occurs by overcoming an activation barrier of 8.4 kcal/mol via **TS_{21-22_OTf}** which forms **22_OTf**. The approach of the *ortho*-carbon of the phenolate to the oxo ligand in **22_OTf** promotes the first redox process via an associative mechanism to afford **23_OTf**.^{10a} The formation of this species (**23_OTf**) is calculated to be exergonic as much as 36.3 kcal/mol, suggesting that the first redox process is not reversible.

The second redox process commences with formation of outer-sphere complex **24** formed by dissociation of the triflate ligand from **23_OTf**. Due to the weakly coordinating nature of the triflate anion, the outer-sphere complex **24** is only 9.1 kcal/mol higher in energy than the inner-sphere complex **23_OTf**. The triflate anion within **24** is then predicted to act as a base and through a deprotonation reaction via **TS₂₄₋₂₅** produces Zwitterion-type complex **25** with an overall activation barrier of 16.2 kcal/mol. The delivery of the resultant triflic acid to the

anionic oxygen of the catecholate ligand within **25** gives **26** (a tautomer of **24**) from which the second redox process proceeds via transition structure **TS₂₆₋₂₇**. The deprotonation of the hydroxy group in **26** by the triflate anion increases the electron density on the catecholate ligand, resulting in two electrons from it being transferred to I(III) center via the curly arrow mechanism (Figure 2). Notably, due to the weakly coordinating nature of the triflate anion, inner-sphere complex **28** is only 4.0 kcal/mol lower in energy than the outer-sphere complex **26**. As such, according to our calculations, the overall activation barrier for the second redox step (via **TS₂₆₋₂₇**) is only 12.3 kcal/mol. The triflic acid generated in the last step then reacts with **9** and, consistent with the experimental observations,⁵ gives diammonium salt **14** in an exergonic fashion. From the foregoing computational data, we conclude that the rate-determining step of this transformation is the first redox step via sequence **21_OTf** → **22_OTf** → **23_OTf** with an activation barrier of 20.8 kcal/mol. This relatively low free energy of activation is in agreement with the experimental observations and explains why the dearomatization reaction by Bi(*4-CO₂Et*bipy)-HVI occurs at room temperature (Table 1).

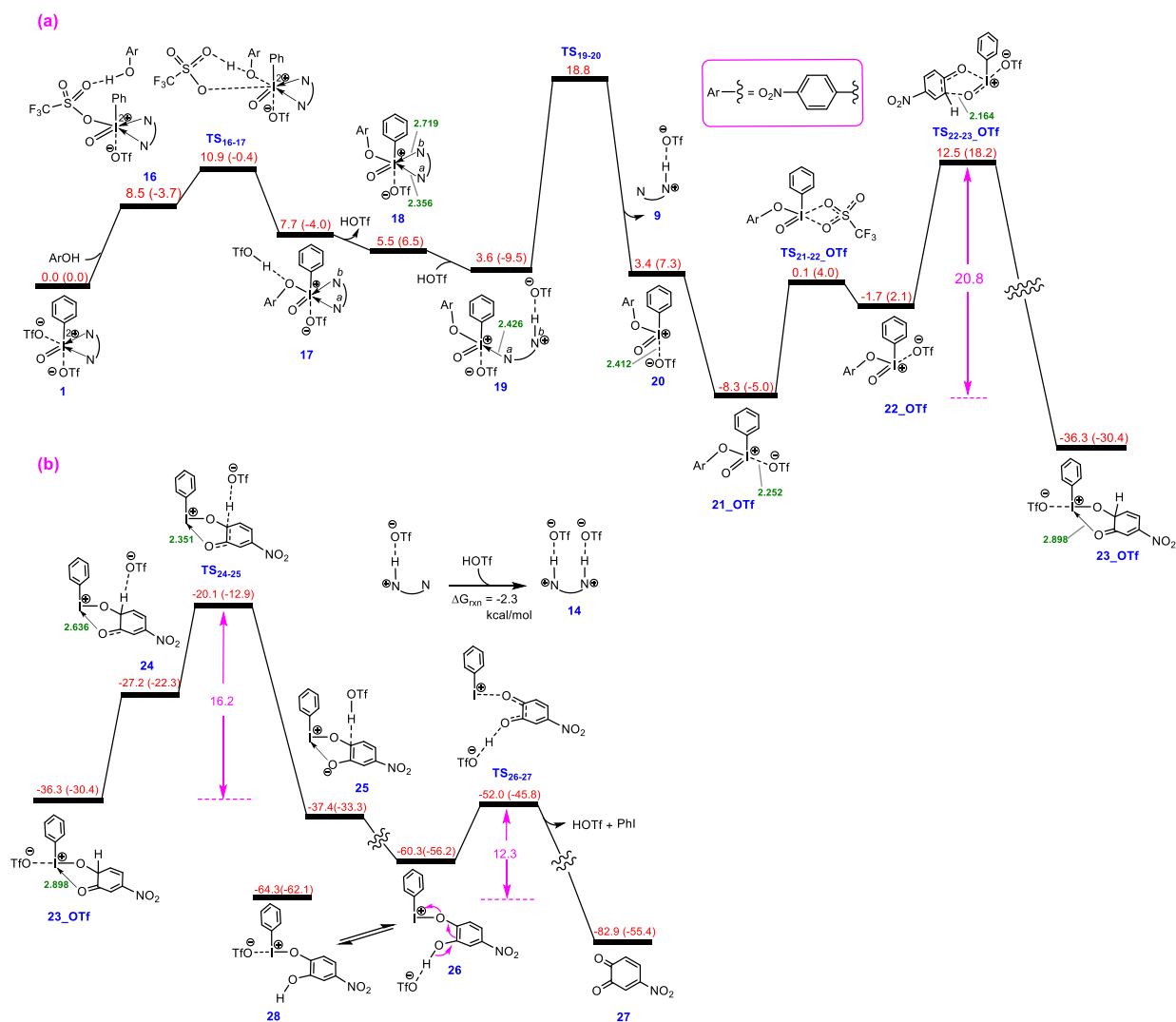


Figure 2. Calculated energy profile for oxidation of *p*-nitrophenol by Bi(4-CO₂Etbipy)-HVI. Free energies (potential energies) calculated by SMD/M06-2X/def2-TZVP//SMD/M06-2X/LANL2DZ(d),6-31G(d) in chloroform are given in kcal/mol and selected bond distances (green values) in Å.

Oxidative dearomatization by PhI(O)(X)₂ (X = OTf, TFA, OAc). It was demonstrated that PhI(O)(OTf)₂ can mediate the oxidation of *p*-nitrophenol, while PhI(O)(OAc)₂ gives no reaction (Table 1, entries 4 and 5).⁵ Furthermore, it was noted that the *ortho*-quinone product formed by reaction with PhI(O)(OTf)₂ decomposed as the reaction time increased (Table 1, entries 6).⁵ This observation suggests that the presence of the Lewis basic bipyridine ligand in Bi(4-CO₂Etbipy)-HVI plays an important role in reducing product degradation. Thus, we employed DFT to investigate and understand the underlying reasons for the reactivity differences between PhI(O)(OTf)₂ and PhI(O)(OAc)₂. For benchmarking purposes, we also

studied the oxidation of *p*-nitrophenol by $\text{PhI}(\text{O})(\text{TFA})_2$ computationally to predict the reactivity of this oxidant. As discussed in the previous section, the first redox process is the rate-determining step of the oxidative dearomatization. Consequently, for these three systems we limited our calculations to studying this part of the reaction mechanism. As shown in Figure 3, the dearomatization commences with the ligand exchange between ArOH and $\text{PhI}(\text{O})(\text{X})_2$ ($\text{X} = \text{OTf}, \text{TFA}, \text{OAc}$) via the CIA mechanism,⁷ followed by a hypervalent twist and then the redox process via the nucleophilic attack of the *ortho*-carbon of the phenolate to the oxo ligand. The computed energy profiles given in Figure 3, revealed several noteworthy points.

(i) The coordinating ability of the X ligand decreases in the following order: $\text{X} = \text{OAc} > \text{TFA} > \text{OTf}$, supported by the shortest I–X bond distance in **29_OAc** (2.101 Å), and the longest one in **29_OTf** (2.141 Å).

(ii) The overall activation barrier for the oxidative dearomatization increases in the order $\text{X} = \text{OTf} < \text{TFA} < \text{OAc}$. This suggests that the identity of the X-ligand is an important factor in determining the ease of the redox process. Specifically, $\text{PhI}(\text{O})(\text{OAc})_2$ bearing strongly coordinating acetate ligands has a barrier of 34.5 kcal/mol, while $\text{PhI}(\text{O})(\text{OTf})_2$, with weakly bound triflate ligands has a computed activation barrier of only 21.7 kcal/mol. This finding is in agreement with the experimental observations and clearly explains why $\text{PhI}(\text{O})(\text{OTf})_2$ is an appropriate oxidant for the dearomatization reaction, while $\text{PhI}(\text{O})(\text{OAc})_2$ gives no reaction.

(iii) The activation barrier for the ligand exchange via **TS₃₀₋₃₁_X** is mainly reliant on the nature of the X-ligand and increases along with the coordinating ability of the X-ligand. This is because it involves a late transition structure, evident from the notable elongation of the I–X bond from **29_X** to **TS₃₀₋₃₁_X** (Figure 3). The stronger the I–X bond, the more destabilized the transition structure **TS₃₀₋₃₁_X**, and the higher the activation barrier to ligand exchange.

(iv) The ligand exchange represents an almost thermoneutral process, regardless of the nature of the X-ligand, which is consistent with the small values calculated for ΔG_1 listed in Table 2.

(v) The hypervalent twist process is more energetic for a stronger coordinating X-ligand. This is supported by the largest value of ΔG_2 for X = OAc and the smallest one for X = OTf (Table 2). This result can be explained by the low tendency of a relatively strong coordinating X-ligand to occupy a position *trans* to the strong σ -donor oxo ligand within **22_X**.

(vi) The energy barrier of the redox step (transformation **22_X** \rightarrow **TS_{22-23_X}**) is particularly sensitive to the nature of the X-ligand. As the coordinating ability of the X-ligand increases, the activation barrier to this step increases (see the ΔG^\ddagger_1 values in Table 2). Consequently, a strong coordinating X-ligand alleviates the electron deficiency of the iodine(V) center in **22_X**, making it less susceptible to be involved in the redox step. This hypothesis finds support from the inspection of the NPA charge on the iodine atom in **22_X**, which increases along the series from +2.544 in **22_OAc** to +2.568 in **22_OTf** (Figure 3). Also, this feature causes the redox step for a relatively strong coordinating X-ligand to take place via a later transition structure (**TS_{22-23_X}**), consistent with the shortest C \cdots O distance in **TS_{22-23_OAc}** (2.125 Å) and the longest one in **TS_{22-23_OTf}** (2.164 Å, Figure 3).

(vii) The overall activation barrier to the first redox process is determined by the following formula: $\Delta G^\ddagger_t = \Delta G_1 + \Delta G_2 + \Delta G^\ddagger_1$ (Table 2). As discussed above, ΔG_1 is mainly independent from the nature of the X-ligand and thus only ΔG_2 and ΔG^\ddagger_1 contribute to the ease of the dearomatization process. A strong coordinating X-ligand makes both transformations **21_X** \rightarrow **22_X** (hypervalent twist) and **22_X** \rightarrow **TS_{22-23_X}** (redox step) unfavorable, and as a result such a ligand is not appropriate for the phenol oxidation.

(viii) The first redox process by PhI(O)(OTf)_2 proceeds with an overall activation energy of 21.7 kcal/mol (Figure 3a), which is comparable to that of 20.8 kcal/mol where the process is driven by $\text{Bi(4-CO}_2\text{Etbipy)-HVI}$ (Figure 2a). This result implies that these two reagents should have a very similar reactivity and the presence of the bipyridine ligand in the latter does not attenuate the oxidizing capacity of the iodine(V) center. This suggests that the presence of the

bipyridine ligand allows for trapping of the in-situ-generated triflic acid, which considerably reduces the rate of decomposition of the sensitive *ortho*-quinone product, as shown in Table 1.

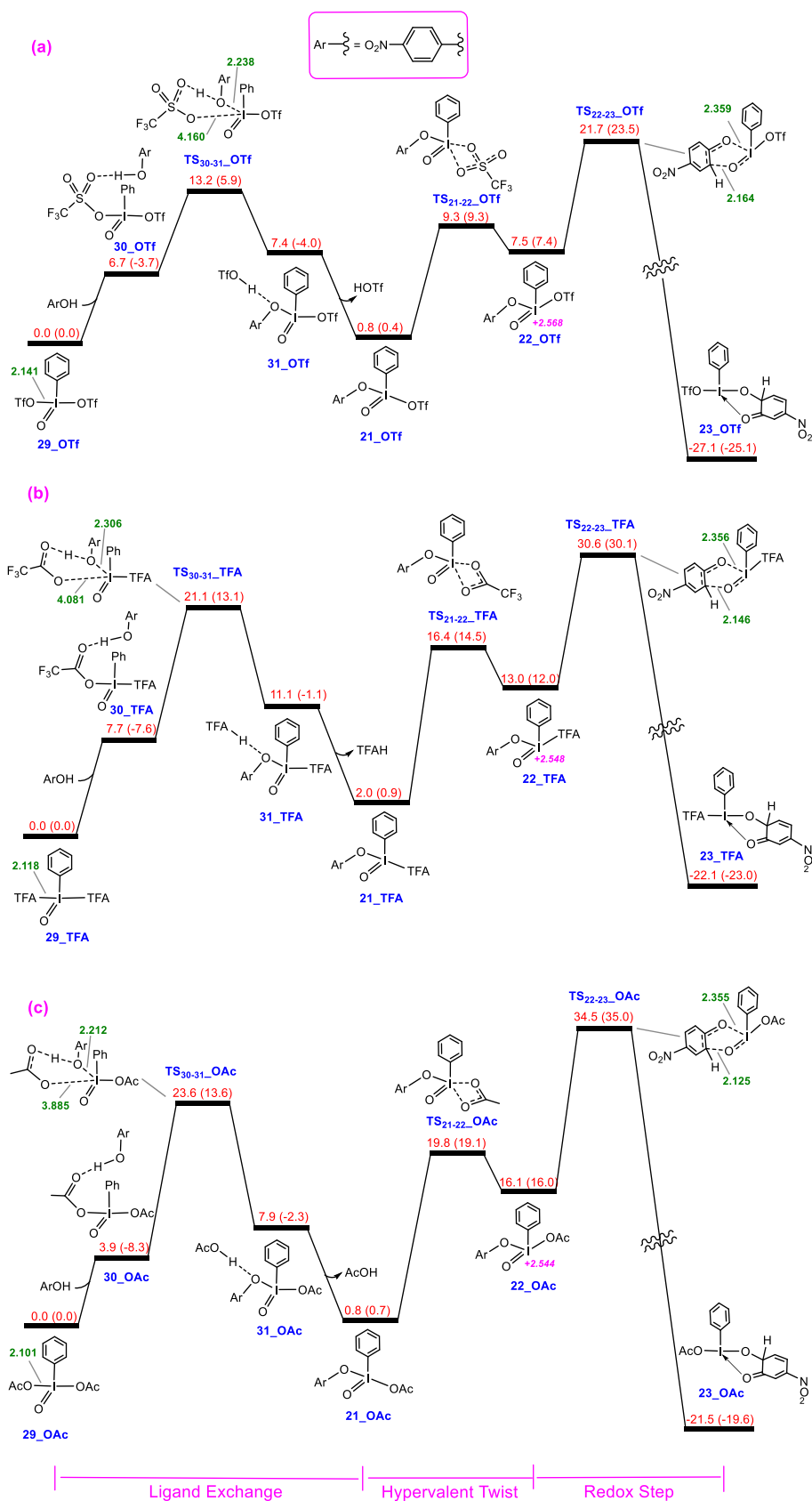
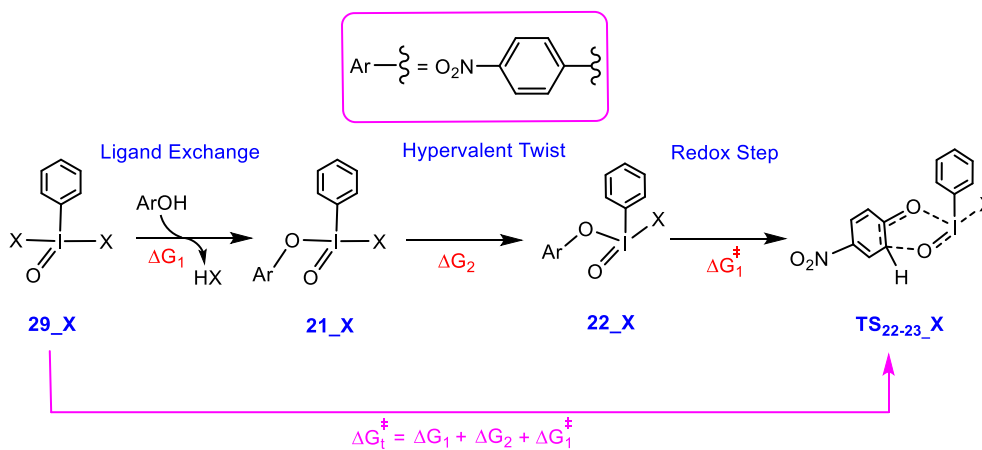


Figure 3. Calculated energy profile for first redox process associated with reaction between **29_X** and ArOH where X = OTf, TFA, and OAc. Free energies (potential energies) calculated by SMD/M06-2X/def2-TZVP//SMD/M06-2X/LANL2DZ(d),6-31G(d) in chloroform are given in kcal/mol and selected bond distances (green values) in Å.

Table 2. Reaction free energies for transformations $29_X \rightarrow 21_X$ (ΔG_1) and $21_X \rightarrow 22_X$ (ΔG_2) and activation free energy for the first redox step (transformation $22_X \rightarrow \text{TS}_{22-23_X}$, ΔG_1^\ddagger). Free energies calculated by SMD/M06-2X/def2-TZVP//SMD/M06-2X/LANL2DZ(d),6-31G(d) in chloroform are given in kcal/mol.



X	ΔG_1	ΔG_2	ΔG_1^\ddagger	ΔG_t^\ddagger
OTf	0.8	6.7	14.2	21.7
TFA	2.0	11.0	17.6	30.6
OAc	0.8	15.3	18.4	34.5

Oxidation of *p*-nitrophenol by IBX. We recently investigated the mechanism of the double oxidation of phenols by IBX.^{10a} Figure 4 depicts the free energy changes for the three key steps outlined in Table 2. The complete energy profile for the IBX-mediated the oxidation of *p*-nitrophenol is provided in the Supporting Information (Figure S5). Consistent with the experimental findings (Table 1), we found that unlike $\text{PhI}(\text{O})(\text{OTf})_2$, the oxidation of *p*-nitrophenol by IBX requires a high overall activation barrier (30.9 kcal/mol).¹¹ Since the carboxylate ligand within IBX coordinates more strongly than the triflate, both the ΔG_2 and ΔG_1^\ddagger values for IBX are computed to be greater than those for $\text{PhI}(\text{O})(\text{OTf})_2$ (**29_OTf**). In addition, the larger ΔG_1 value for IBX than $\text{PhI}(\text{O})(\text{OTf})_2$ indicates that the former is thermodynamically more resistant to ligand exchange. It follows from these results that all three key steps (ligand exchange,

hypervalent twist, and the redox step) contribute to the much lower reactivity of IBX toward oxidation of electron-deficient phenols.

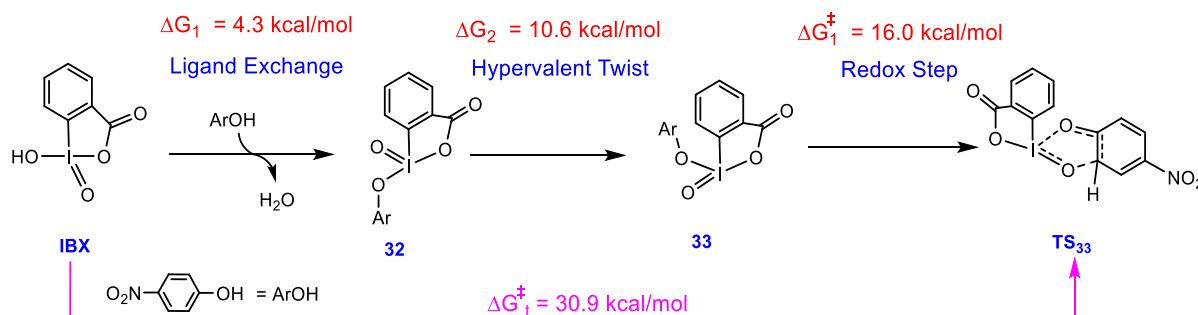


Figure 4. Reaction free energies for the oxidation of *p*-nitrophenol by IBX. Free energies calculated by SMD/M06-2X/def2-TZVP//SMD/M06-2X/LANL2DZ(d),6-31G(d) in chloroform are given in kcal/mol.

Oxidation of *p*-nitrophenol by $\text{PhI}(\text{O})(\text{Py})_2(\text{OTf})_2$. It was determined experimentally that substituting the bidentate bipyridine ligand with two pyridine ligands results in deactivation of the Bi(*N*)-HVI oxidant and recovery of the starting material (Table 1, entry 8).⁵ This can be probed by DFT, which predicts that geometrical isomer **36** is ~12 kcal/mol more stable than the active oxidant **34** (Figure 5). The latter is produced only after surmounting an activation barrier as high as 27.7 kcal/mol. The most stable isomer **34** is not reactive toward the ligand exchange process because the two active sites in this complex are blocked by the pyridine ligands. Specifically, in the most stable structure, the triflate ligands responsible for driving the ligand exchange occupy positions *trans* to the strong σ -donor phenyl and oxo ligands which renders this complex incapable of facilitating the oxidation. This hypothesis is supported by the highly unstable nature of intermediates **37** and **38** resulting from ligand exchange between **34** and ArOH. To summarize, the high stability of the inactive iodine(V) complex **34** does not allow ligand exchange to easily occur on such a system, and this is the likely reason for no reaction occurring between $\text{PhI}(\text{O})(\text{Py})_2(\text{OTf})_2$ and *p*-nitrophenol.¹¹

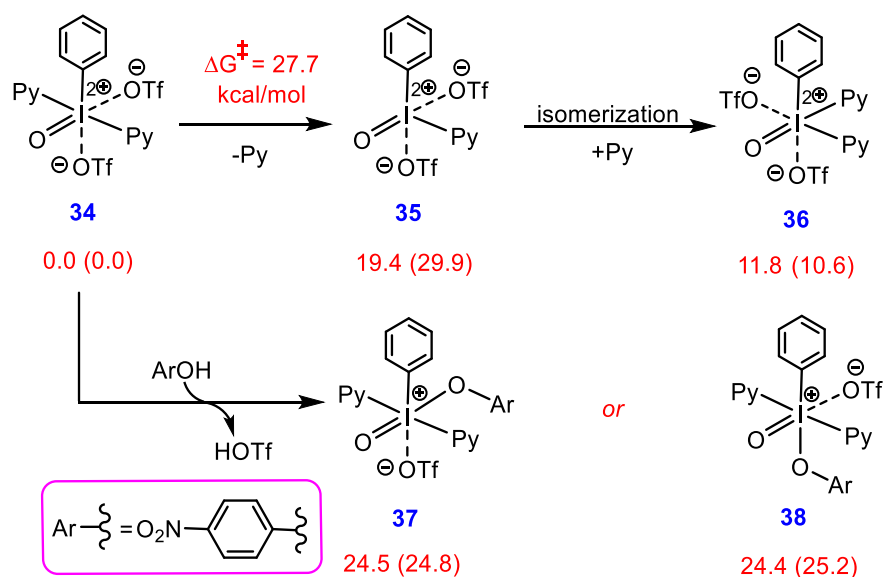


Figure 5. Calculated mechanism for generation of active oxidant **36** from the most stable isomer **34** along with the relative energy of intermediates **37** and **38** achieved by ligand exchange reaction between **34** and *p*-nitrophenol (ArOH). Free energies (potential energies) calculated by SMD/M06-2X/def2-TZVP//SMD/M06-2X/LANL2DZ(d),6-31G(d) in chloroform are given in kcal/mol.

Oxidation of *p*-nitro-phenol by Bi(4-OMebipy)-HVI. Finally, we wanted to understand why the yield of the oxidative reaction is reduced by replacing the 4,4'-ester substituents within Bi(4-CO₂Etbipy)-HVI with strongly electron-donating 4,4'-dimethoxy moieties (Table 1, entries 1 and 7).⁵ From the DFT-derived mechanism illustrated in Scheme 1, we posit that the reaction between *p*-nitrophenol and Bi(4-OMebipy)-HVI should commence with the ligand exchange followed by protonation of the bipyridine ligand to give **19_OME** (Figure 6). The overall activation free energy for these two key steps is computed to be only 10.1 kcal/mol.¹¹ Based on the proposed mechanism, for the redox process to proceed, the protonated bipyridine ligand needs to dissociate from **19_OME** to give key intermediate **22_OTf**. The presence of the electron-donating 4,4'-dimethoxy groups on the bipyridine ligand cause this key step to take place with an activation barrier of 25.1 kcal/mol, which is much more energy demanding in comparison to analogous process from **19** (18.8 kcal/mol, Figure 2a). The stronger coordination of the bipyridine ligand within **19_OME** than in **19** is evident from the shorter I–N bond distance in the former (2.336 Å) than in the latter (2.426 Å) (see Figures 6 and 2a).

Consequently, Bi(4-OMebipy)-HVI is less reactive than Bi(4-CO₂Etbipy)-HVI toward the phenol oxidation, likely because the more tightly coordinated 4,4'-methoxy bipyridine ligand retards the formation of key intermediate **22_OTf**.

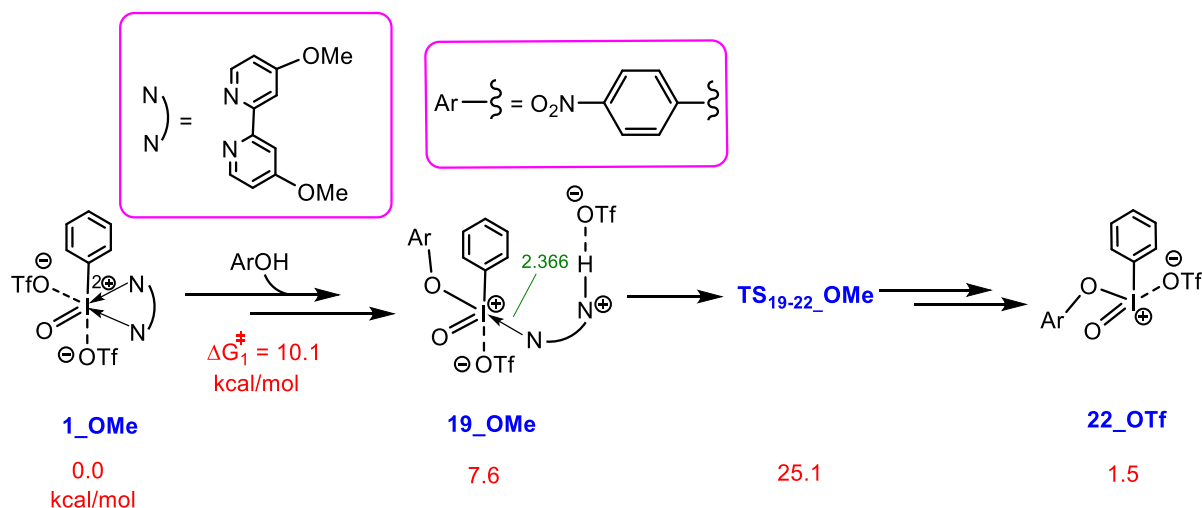


Figure 6. Calculated mechanism for formation of the key intermediate **22_OTf** from reaction between **1_OMe** and *p*-nitrophenol (ArOH). Free energies calculated by SMD/M06-2X/def2-TZVP//SMD/M06-2X/LANL2DZ(d),6-31G(d) in chloroform are given in kcal/mol.

CONCLUSION

In summary, our comprehensive computational investigation reveals how the key structural and electronic properties of Bi(4-CO₂Etbipy)-HVI facilitate its enhanced oxidation capacity relative to more traditional hypervalent iodine(V) species. We anticipate that these findings will assist in the design and development of new hypervalent iodine(V) reagents and synthetic transformations.

COMPUTATIONAL METHODS

Gaussian 16¹² was used to fully optimize all the structures reported in this paper at the M06-2X level¹³ of density functional theory (DFT). For all the calculations, solvent effects were considered using the SMD solvation model for CHCl₃ solvent.¹⁴ The effective core potential of

Hay and Wadt with a double- ξ valence basis set (LANL2DZ)¹⁵ was chosen to describe iodine. Polarization functions were also added for I ($\xi_d = 0.289$).¹⁶ The 6-31G(d) basis set was used for other atoms.¹⁷ This basis set combination will be referred to as BS1. Frequency calculations were carried out at the same level of theory as those for the structural optimization. Transition structures were located using the Berny algorithm. Intrinsic reaction coordinate (IRC) calculations¹⁸ were used to confirm the connectivity between transition structures and minima. To further refine the energies obtained from the SMD/M06-2X /BS1 calculations, we carried out single-point energy calculations using the M06-2X functional method¹⁹ for all the structures with a larger basis set (BS2). BS2 utilizes def2-TZVP²⁰ basis set on all atoms. Tight convergence criterion was also employed to increase the accuracy of the single point calculations. All thermodynamic data were calculated at the standard state (298.15 K and 1 atm).

In this work, the free energy for each species optimized by SMD/M06-2X/BS1 in solution was calculated using the formula: $G = E(\text{BS2}) + G(\text{BS1}) - E(\text{BS1}) + \Delta G^{1\text{atm} \rightarrow 1\text{M}}$, where $\Delta G^{1\text{atm} \rightarrow 1\text{M}} = 1.89$ kcal/mol is the free-energy change for compression of 1 mole of an ideal gas from 1 atm to the 1 M solution phase standard state. Natural population analysis (NPA) was carried out using NBO6 software integrated into Gaussian 16.²¹

The free energy barriers for ligand dissociation via **TS₁₉₋₂₀**, **TS₃₄₋₃₅**, **TS₁₈₋₂₀** and **TS_{19-22-OMe}** were estimated according to the protocol presented by Hall and Hartwig.²² In this protocol, for example, the Gibbs free energy barrier for a dissociation reaction such as $A-B \rightarrow A + B$ is estimated as $\Delta G^\ddagger \approx \Delta H = H_A + H_B - H_{A-B}$.

ASSOCIATED CONTENT

Supporting Information

The Supporting Information is available free of charge on the ACS Publications website.

AUTHOR INFORMATION

Corresponding Authors

*E-mail: Alireza.Ariafard@utas.edu.au.

orcid.org/0000-0003-2383-6380

*E-mail: SarahW@temple.edu.

orcid.org/0000-0002-4797-0181

Notes

The authors declare no competing financial interest.

ACKNOWLEDGMENTS

We thank the Australian Research Council (ARC) for project funding (DP180100904) and the Australian National Computational Infrastructure and the University of Tasmania for the generous allocation of computing time. A.C.B.'s contributions were supported by an ARC Future Fellowship (FT200100049).

REFERENCES

- (1) (a) Zhdankin, V. V.; Stang, P. J. Chemistry of Polyvalent Iodine. *Chem. Rev.* **2008**, 108, 5299-5358. (b) Charpentier, J.; Fruh, N.; Togni, N. A. electrophilic Trifluoromethylation by Use of hypervalent Iodine Reagents. *Chem. Rev.* **2015**, 115, 650-682. (c) Yoshimura, A.; Yusubov, M.; Zhdankin, V. V. Synthetic applications of Pseudocyclic Hypervalent Iodine compounds. *Org. Biomol. Chem.* **2016**, 14, 4771-4781. (d) Kohlhepp, S. V.; gulder, T. Hypervalent Iodine (III) Fluorinations of Alkenes and Diazo compounds: New Opportunities in fluorination chemistry. *Chem. Soc. Rev.* **2016**, 45, 6270-6288. (e) Yoshimura, A.; Zhdankin, V. V. Advances in Synthetic Applications of Hypervalent Iodine compounds. *Chem. Rev.* **2016**, 116, 3328-3435.
- (2) (a) Ladziata, U.; Zhdankin, V. V. Hypervalent Iodine (V) Reagents in Organic synthesis. *Arkivoc.* **2006**, ix, 26-58. (b) Satam, V.; Harad, A.; Rajule, R.; Pati, H. 2-Iodoxybenzoic acid (IBX): an Efficient Hypervalent Iodine Reagent. *Tetrahedron.* **2010**, 66, 7659-706. (c) Zhdankin, V. V. Organoiodine (V) Reagents in Organic Synthesis. *J. Org. Chem.* **2011**, 76, 1185-1197. (d) Duschek, A.; Kirsch, S. F. 2-Iodoxybenzoic acid-A Simple Oxidant with a Dazzling Array of Potential Applications. *Angew. Chem. Int. Ed.* **2011**, 50, 1524-1552. (e) Bernini, R.; Fabrizi, G.; Pouysegue, L.; Defiieux, D.; Quideau, S. Synthesis of biologically Active Catecholic Compounds via ortho-Selective Oxygenation of Phenolic Compounds Using Hypervalent Iodine (V) Reagents. *Curr. Org. Synth.* **2012**, 9, 650-669.
- (3) For the first example of a regioselective ortho-quinone synthesis using IBX, see: a) Magdziak, M.; rodriguez, R. W.; De Water, R. W.; Petus, T. R. R. *Org. Lett.* **2002**, 4, 285-28. b) Tohma, h.; Kita, Y. Hypervalent Iodine Reagents for Oxidation of alcohols and their application to complex molecule synthesis. *Adv. Synth. Catal.* **2004**, 346, 111. (c) Uyanik, M.; Mutsuga, T.; Ishihara, K. *Angew. Chem. Int. Ed.* **2017**, 56, 3956-3960. (d) Stack, D. E.; Mahmud, B. *Synth. Commun.* **2018**, 48, 161-167.
- (4) Zhdankin, V. V.; Kuposov, A. Y.; Yashin, N. V. complexes of Hypervalent Iodine Compounds with nitrogen Ligands. *Tetrahedron Lett.* **2002**, 43, 5735-5737.
- (5) Xiao, X.; Greenwood, N. S.; Wengriniuk, S. E. Dearomatization of electron-deficient Phenols to ortho-Quinones: Bidentate Nitrogen-Ligated Iodine(V) Reagents. *Angew. Chem. Int. Ed.* **2019**, 58, 16181-16187.

- (6) Xiao, X.; Roth, J. M.; Greenwood, N. S.; Veloplcek, M. K.; Aquirre, J.; Jalali, M.; Ariaifard, A.; Wengryniuk, S. E. Bidentate Nitrogen-Ligated I(V) Reagents, Bi(N)-HVI: Preparation, stability, structure, and Reactivity. *J. Org. Chem.* **2021**, *86*, 6566-6576.
- (7) (a) Ganji, B.; Ariaifard, A. DFT Mechanistic Investigation into Phenol Dearomatization Mediated by an Iodine (III) Reagent. *Org. Biomol. Chem.* **2019**, *17*, 3521-3528. (b) Farshadfar, K.; Chipman, A.; Yates, B. F.; Ariaifard, A. DFT Mechanistic Investigation into BF₃-catalyzed Alcohol Oxidation by a hypervalent Iodine (III) Compound. *ACS. Catal.* **2019**, *9*, 6510-6521.
- (8) The dissociation of the bipyridine ligand from **18** gives **20** with a relative energy of 26.1 kcal/mol and occurs with an overall activation barrier of ~31.6 kcal/mol, indicating that the protonation of the N^b atom by triflic acid is particularly necessary for the bipyridine ligand to be liberated more easily.
- (9) (a) Su, J. T.; Goddard, W. A. Enhancing 2-Iodoxybenzoic Acid Reactivity by Exploiting a Hypervalent Twist. *J. Am. Chem. Soc.* **2005**, *127*, 14146-14147. (b) Jiang, H.; Sun, T. Y.; Wang, X.; Xie, Y.; Zhang, X.; Wu, Y. D.; Schaefer, H. F. A Twist of the Twist Mechanism, 2-Iodoxybenzoic Acid (IBX)-Mediated Oxidation of Alcohol Revisited: theory and Experiment. *Org. Lett.* **2017**, *19*, 6502-6505.
- (10) Kaur, A.; Ariaifard, A. Mechanistic Investigation into Phenol Oxidation by IBX Elucidated by DFT Calculations. *Org. Biomol. Chem.* **2020**, *18*, 1117-1129.
- (11) For the full energy profile, see the Supporting Information.
- (12) Gaussian 16, Revision B.01, Frisch, M. J.; Trucks, G. W.; Schlegel, H. B.; Scuseria, G. E.; Robb, M. A.; Cheeseman, J. R.; Scalmani, G.; Barone, V.; Petersson, G. A.; Nakatsuji, H.; Li, X.; Caricato, M.; Marenich, A. V.; Bloino, J.; Janesko, B. G.; Gomperts, R.; Mennucci, B.; Hratchian, H. P.; Ortiz, J. V.; Izmaylov, A. F.; Sonnenberg, J. L.; Williams-Young, D.; Ding, F.; Lipparini, F.; Egidi, F.; Goings, J.; Peng, B.; Petrone, A.; Henderson, T.; Ranasinghe, D.; Zakrzewski, V. G.; Gao, J.; Rega, N.; Zheng, G.; Liang, W.; Hada, M.; Ehara, M.; Toyota, K.; Fukuda, R.; Hasegawa, J.; Ishida, M.; Nakajima, T.; Honda, Y.; Kitao, O.; Nakai, H.; Vreven, T.; Throssell, K.; Montgomery, J. A.; Peralta, J. E.; Ogliaro, F.; Bearpark, M. J.; Heyd, J. J.; Brothers, E. N.; Kudin, K. N.; Staroverov, V. N.; Keith, T. A.; Kobayashi, R.; Normand, J.; Raghavachari, K.; Rendell, A. P.; Burant, J. C.; Iyengar, S. S.; Tomasi, J.; Cossi, M.; Millam, J. M.; Klene, M.; Adamo, C.; Cammi, R.; Ochterski, J. W.; Martin, R. L.; Morokuma, K.; Farkas, O.; Foresman, J. B.; and Fox, D. J. Gaussian, Inc., Wallingford CT, **2016**.
- (13) (a) Lee, C. T.; Yang, W. T.; Parr, R. G. Development of the Colic-Salvetti Correlation-energy Formula into a Functional of the Electron Density. *Phys. Rev. B.* **1988**, *37*, 785-789; (b) Miehlich, B.; Savin, A.; Stoll, H.; Preuss, H. Results Obtained with the Correlation Energy Density Functionals of Becke and Lee, Yang and Parr. *Chem. Phys. Lett.* **1989**, *157*, 200-206; (c) Becke, A. D. J. Density Functional Thermochemistry.III. The Role of Exact Exchange. *Chem. Phys.* **1993**, *98*, 5648-5652.
- (14) Marenich, A. V.; Cramer, C. J.; Truhlar, D. G. Universal Solvation Model Based on Solute Electron Density and on a continuum Model of the Solvent defined by the Bulk Dielectric Constant and Atomic Surface Tensions. *J. Phys. Chem. B.* **2009**, *113*, 6378-6396.
- (15) (a) Hay, P. J.; Wadt, W. R. Ab initio Effective Core Potentials for Molecular Calculations. Potentials for the Transition Metal Atoms Sc to Hg. *J. Chem. Phys.* **1985**, *82*, 270-283. (b) Wadt, W. R.; Hay, P. J. Ab initio Effective Core Potentials for Molecular Calculations. Potentials for Main Group elements Na to Bi. *J. Chem. Phys.* **1985**, *82*, 284-298.
- (16) Ehlers, A. W.; Dapprich, M. S.; Gobbi, A.; Höllwarth, A.; Jonas, V.; Köhler, K. F.; Stegmann, R.; Veldkamp, A.; Frenking, G. A Set of f-polarization Functions for Pseudo-potential Basis Sets of the Transition Metals Sc, Cu, Y, Ag, La, Au. *Chem. Phys. Lett.* **1993**, *208*, 111-114.
- (17) Hariharan, P. C.; Pople, J. A. The Influence of Polarization Functions on Molecular Orbital Hydrogenation Energies. *Theor. Chim. Acta J. A.* **1973**, *28*, 213-222.
- (18) (a) Fukui, K. J. Formulation of the Reaction coordinate. *Phys. Chem.* **1970**, *74*, 4161-4163; (b) Fukui, K. The Path of The Chemical Reactions -The IRC Approach. *Acc. Chem. Res.* **1981**, *14*, 363-368.
- (19) Zhao, Y.; Truhlar, D. G. Density Functionals with Broad Applicability in Chemistry. *Acc. Chem. Res.* **2008**, *41*, 157-167.
- (20) Weigend, F.; Furche, F. and Ahlrichs, R. J. Gaussian Basis Sets of Quadruple Zeta Valence Quality for Atoms H-Kr. *Chem. Phys.* **2003**, *119*, 12753-12762.
- (21) Glendening, E. D.; Badenhoop, J. K.; Reed, a. E.; Carpenter j. E.; Bohmann, J. A.; Morales, C. M.; Landis, C. R.; Weinhold, F. Natural Bond Order 6.0, *Theoretical Chemistry Institute, University of Wisconsin, Madison, WI*, **2013**, <http://nbo6.chem.wisc.edu>.
- (22) Hartwig, J. F.; Cook, K. S.; Hapke, M.; Incarvito, C. D.; Fan, Y.; Webster, C. E.; Hall, M. B. Rhodium Boryl Complexes in the Catalytic, Terminal Functionalization of Alkanes. *J. Am. Chem. Soc.* **2005**, *127*, 2538-2552.